its oxidation state, and the presence of hydrogen-bonding interactions.[19] The 416-cm^{-1} feature is tentatively assigned to a metal-ligand vibration coupled to the Fe–O stretch.[20]

Species **2** exhibits an EPR spectrum (Figure 2) with principal **g** values at $g_x = 3.95$, $g_y = 4.40$, and $g_z \sim 2.00$, assigned to the ground Kramers doublet ($S' = {}^1/_2$) of a system with half-integral spin. Its intensity accounts for as much as 0.47 spin/Fe and correlates well with the intensity of the 614-nm band. The EPR spectrum is reminiscent of an $S = {}^3/_2$ multiplet with zero field splitting parameters $D > 0$ and $E/D = 0.04$. The Mössbauer spectra shown in Figure 3 were obtained after treating **1** with 5 equiv of H_2O_2. Approximately 65% of the iron is diamagnetic and consists of two unresolved doublets ($\Delta E_{Q_1} = 1.63$ mm/s, $\Delta E_{Q_2} = 1.15$ mm/s, and $\delta_1 = \delta_2 = 0.44$ mm/s at 140 K). The remainder (ca. 30%) belongs to Kramers species **2**. At 140 K the spectrum of **2** consists of *one* quadrupole doublet (Figure 3a) with $\Delta E_Q = 0.53$ mm/s and $\delta = 0.07$ mm/s. Relative to **1**, the isomer shift of **2** has changed from 0.42 mm/s to 0.07 mm/s, showing that **2** is oxidized relative to **1**, most probably to the Fe(IV) state. In fact, the observed value of δ is similar to those of Fe(IV) complexes in heme[21] and non-heme[22] environments. At 4.2 K, **2** exhibits paramagnetic hyperfine structure (solid line in Figure 3b) as expected for a Kramers species and has a magnetic field dependence (60 mT $\perp$ vs 60 mT $\parallel$) predictable from the EPR spectrum (solid line in Figure 3c).[23] The EPR spectrum of the Mössbauer sample accounts for 0.3 spin/Fe. Since 30% of the ^{57}Fe Mössbauer absorption is associated with **2**, the EPR and Mössbauer data, taken together, strongly suggest that **2** is a *mononuclear* rather than a dinuclear complex.[24]

The spectroscopic data lead us to postulate the following reaction scheme:

$$\underset{\mathbf{1}}{[\mathrm{LFe{-}O{-}FeL}]^{4+}} + \mathrm{H_2O_2} \rightarrow \underset{\mathbf{2}}{[\mathrm{LFeO}]^{3+}} + \underset{\mathbf{3}}{[\mathrm{LFeOH}]^{2+}} + \mathrm{OH^-}$$

In this scheme, treatment of **1** with H_2O_2 causes the 2e oxidation of one of the ferric ions. Subsequent cleavage of the dinuclear complex yields **2** and ferric complex **3**; the latter then dimerizes to form the spin-coupled diferric complex of parts a and b of Figure 3, which does not react with H_2O_2 at -40 °C. Thus, a stoichiometric formation of **2** would correspond to a maximum of 0.5 spin/Fe. It is clear from the spectroscopic data that **2** is a novel species; it is a Kramers system containing the non-Kramers ion Fe(IV) and exhibits remarkably small magnetic hyperfine interactions. These unusual observations can be reconciled with a model that considers ferromagnetic coupling ($H = JS_1{\cdot}S_2$, $J < 0$) of an $S = 1$ ferryl complex[25] ($D > 15$ cm^{-1}, $E/D = 0.04$) to an $S = {}^1/_2$ radical, with coupling strength $J/D \sim -1.5$.[26] We therefore formulate **2** as $[(\mathrm{L}^{\bullet+})\mathrm{Fe^{IV}{=}O}]^{3+}$, a species with electronic features similar to those of heme peroxidase compounds I[1a,27] and related to the putative $[(\mathrm{Por})\mathrm{Fe(O)}]^+$ species in cytochrome P-450.[2] Thus high-valent iron-oxo species may also play a crucial role in the alkane functionalization reactions catalyzed by non-heme iron centers.

Acknowledgment. This work was supported by grants from the National Institutes of Health to L.Q. (GM-33162) and E.M. (GM-22701). We acknowledge an NIH National Research Service Award to R.A.L. (GM-13343) and an NIH Predoctoral Traineeship to B.A.B. (GM-08277).

---

[19] (a) Paeng, K.-J.; Kincaid, J. R. *J. Am. Chem. Soc.* **1988**, *110*, 7913–7915. (b) Terner, J.; Sitter, A. J.; Reczek, C. M. *Biochim. Biophys. Acta* **1985**, *828*, 73–80. (c) Kincaid, J. R.; Schneider, A. J.; Paeng, K.-J. *J. Am. Chem. Soc.* **1989**, *111*, 735–737. (d) Czernuszewicz, R.; Su, Y. O.; Stern, M. K.; Macor, K. A.; Kim, D.; Groves, J. T.; Spiro, T. G. *J. Am. Chem. Soc.* **1988**, *110*, 4158–4165. (e) Su, Y. O.; Czernuszewicz, R.; Miller, L. A.; Spiro, T. G. *J. Am. Chem. Soc.* **1988**, *110*, 4150–4157. (f) Nick, R. J.; Ray, G. B.; Fish, K. M.; Spiro, T. G.; Groves, J. T. *J. Am. Chem. Soc.* **1991**, *113*, 1838–1840.

[20] (a) Attempts to fit the 416- and 666-cm^{-1} bands as ν_s and ν_{as}, respectively, of an Fe–O–Fe or related unit were unsuccessful. (b) In the resonance Raman spectrum of hemerythrin, a band at 292 cm^{-1} displaying a 6-cm^{-1} ^{18}O shift has been assigned to an Fe–N(imidazole) stretch coupled to an Fe–O bond; see: Czernuszewicz, R. S.; Sheats, J. E.; Spiro, T. G. *Inorg. Chem.* **1987**, *26*, 2063–2067 and references therein.

[21] See Table I in the following: Schulz, C. E.; Rutter, R.; Sage, J. T.; Debrunner, P. G.; Hager, L. P. *Biochemistry* **1984**, *23*, 4743–4754.

[22] Collins, T. J.; Kostka, K. L.; Münck, E.; Uffelman, E. S. *J. Am. Chem. Soc.* **1990**, *112*, 5637–5639.

[23] Münck, E.; Huynh, B. H. *ESR and NMR of Paramagnetic Species in Biological and Related Systems*; Bertini, I., Drago, R. S., Eds.; D. Reidel: Amsterdam, 1979; pp 275–288.

[24] Other Mössbauer samples, produced with different H_2O_2 concentrations, give essentially the same spectroscopic results; in all cases, the concentration of **2** obtained from EPR agrees with that obtained from the Mössbauer studies. Thus, the spectroscopic properties of **2** do not depend on the H_2O_2 concentration.

[25] Oosterhuis, W. T.; Lang, G. *J. Chem. Phys.* **1973**, *58*, 4757–4765.

[26] The **g** and **A** tensors of the Fe(IV) t_{2g}^4 configuration were taken from ref 25 for $\Delta/\zeta = 3.7$ and $V/\Delta = -0.1$ where Δ and V are the tetragonal and rhombic ligand field parameters and ζ is the spin-orbit coupling constant ($\sim$400 cm^{-1}). Although the EPR spectrum resembles that observed for $S = {}^3/_2$ multiplets, the EPR ($g_\perp > 4$) and Mössbauer (small **A** values) data are in conflict with either a d^3 $S = {}^3/_2$ Fe(V) or a strongly coupled ($|J| > |D|$) $S = {}^3/_2$ system. Details will be reported elsewhere.

[27] Rutter, R.; Hager, L. P.; Dhonau, H.; Hendrich, M. P.; Valentine, M.; Debrunner, P. *Biochemistry* **1984**, *23*, 6809–6816.

Distortion toward Bridging Accompanying Hyperconjugation in a Simple Tertiary Alkyl Carbocation

Paul von Rague Schleyer* and José W. de M. Carneiro

Institut für Organische Chemie
Universität Erlangen-Nurnberg, Henkestrasse 42
D-8520 Erlangen, Federal Republic of Germany

Wolfram Koch

Heidelberg Scientific Center, IBM Deutschland GmbH
Tiergartenstrasse 15, D-6900 Heidelberg
Federal Republic of Germany

David A. Forsyth*

Department of Chemistry, Northeastern University
Boston, Massachusetts 02115

Received July 30, 1990

The 2-methyl-2-butyl (*tert*-pentyl) cation is the smallest tertiary carbocation that affords the possibility of stabilization through C–C hyperconjugation. The cation could adopt structure **1**, in which the C3–C4 bond is aligned parallel with the "vacant" p orbital at C2$^+$, or the planar geometry, **2**, in which C–C hyperconjugation cannot take place. Despite experimental measurement of a variety of properties,[1-6] detailed information concerning the structure of the *tert*-pentyl cation has been completely lacking. The *tert*-pentyl cation has long been assumed to be "classical", and the NMR chemical shifts have been taken as references for carbenium ion behavior.[1-4] This assumption requires significant refinement, as we will demonstrate in this paper through the use of ab initio structures and IGLO (*i*ndividual *g*auge for *l*ocalized molecular *o*rbitals) chemical shift calculations. Specifically, geometrical distortion toward bridging accompanies C–C hyperconjugation and leads to a reduction of about 20 ppm in the

---

[1] (a) Olah, G. A.; Baker, E. B.; Evans, J. C.; Tolgyesi, W. S.; McIntyre, J. S.; Bastein, I. J. *J. Am. Chem. Soc.* **1964**, *86*, 1360. (b) Olah, G. A.; Lukas, J. *J. Am. Chem. Soc.* **1967**, *89*, 4739. (c) Olah, G. A.; Donovan, D. J. *J. Am. Chem. Soc.* **1977**, *99*, 5026. (d) Olah, G. A.; Donovan, D. J. *J. Am. Chem. Soc.* **1978**, *100*, 5163.

[2] (a) Saunders, M.; Hagen, E. L. *J. Am. Chem. Soc.* **1968**, *90*, 2436. (b) Saunders, M.; Vogel, P.; Hagen, E. L.; Rosenfeld, J. *Acc. Chem. Res.* **1973**, *6*, 53 and references therein. (c) Saunders, M.; Budiansky, S. P. *Tetrahedron* **1979**, *35*, 929.

[3] Servis, K. L.; Shue, F.-F. *J. Am. Chem. Soc.* **1980**, *102*, 7233.

[4] Schleyer, P. v. R.; Lenoir, D.; Mison, P.; Liang, G.; Prakash, G. K. S.; Olah, G. A. *J. Am. Chem. Soc.* **1980**, *102*, 683 and references therein.

[5] (a) Solomon, J. J.; Field, F. H. *J. Am. Chem. Soc.* **1973**, *95*, 4483. (b) Solomon, J. J.; Meot-Ner, M.; Field, F. H. *J. Am. Chem. Soc.* **1974**, *96*, 3727.

[6] Mirda, D.; Rapp, D.; Kramer, G. M. *J. Org. Chem.* **1979**, *44*, 2619.

0002-7863/91/1513-3990$02.50/0

Table I. Relative Energies (kcal/mol) of *tert*-Pentyl Isomers

method (basis//geometry level)	1	2	3
HF/3-21G//HF/3-21G	0.00	1.78	2.49
HF/6-31G*//HF6-31G*	0.00 (0)[a]	0.63 (1)[a]	2.45 (1)[a]
MP2(FU)/6-31G*//MP2(FU)/6-31G*	0.00	0.87	1.17
MP2/6-31G**//MP2(FU)/6-31G*	0.00	0.92	1.14
MP3/6-31G**//MP2(FU)/6-31G*	0.00	0.30	1.70
MP4(sdtq)/6-31G**//MP2(FU)/6-31G*	0.00	0.67	1.46
zero-point energy (ZPE)[b]	98.36	97.64	98.20
final + ZPE (scaled by 0.89)	0.00	0.03	1.32

[a] Number of imaginary frequencies in frequency calculation. [b] ZPE (kcal/mol) calculated by using the HF/6-31G* approach.

^{13}C chemical shift of the C$^+$ carbon compared to structures without partial C–C bridging.

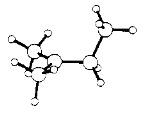

1

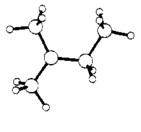

2

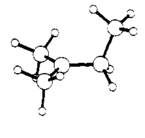

3

We examine here three principal structures for the *tert*-pentyl cation: **1**, **2**, and a methyl-rotated form, **3**. The ab initio calculations were carried out by using the Gaussian 82 or 86 programs.[7] Geometry optimizations were carried out at 3-21G//3-21G, 6-31G*//6-31G* and at the correlated MP2(FU)/6-31G*//MP2(FU)6-31G* levels.[8] The series of geometry optimizations with fixed CCC$^+$ angles for the 1-propyl and *tert*-pentyl cations employed the 3-21G basis set; C_s symmetry was assumed, but all other parameters were allowed to optimize fully. All these geometries were employed for IGLO chemical shift calculations using the standard double ζ (DZ) basis set.[9] The *tert*-pentyl energies were refined up to MP4stdq/6-31G**//MP2(FU)6-31G*+ZPE, our "final" level. The zero-point energies (ZPE) were obtained by frequency calculations at HF/6-31G* and were scaled by 0.89 following the recommended practice.[8] Table I lists the relative energies at the various calculational levels. Table II summarizes the IGLO ^{13}C chemical shift results.

The relative energies of the principal isomers of the *tert*-pentyl cation depend on the theoretical level. At HF/6-31G*, **2** is a transition structure for the 180° rotation of the ethyl group in **1**. Even at this HF level, the barrier is less than 1 kcal/mol; optimizations including correlation at the MP2(FU) level and MP4 single points result in little change (Table I). However, ZPE favors **2**, and its final energy is only 0.03 kcal/mol higher than that of **1**. Hence, both forms are predicted to be equally stable in the gas phase. Conformation **3** is not a minimum, but a transition structure for methyl rotation of **1**, with the final value of the barrier at 1.3 kcal/mol (Table I).

Despite the similar energies predicted for **1**–**3**, a clear-cut decision for **1** as the structure of the *tert*-pentyl cation in solution can be reached by comparing the chemical shifts calculated by IGLO with experiment (Table II). ^{13}C shifts for the carbenium ion center, C2$^+$, are quite revealing, as these shifts vary widely with structure. The IGLO results for C2$^+$ using the MP2(FU)/6-31G* geometries of **1**, **2**, and **3** show no difference from experiment for **1**, but over 17 ppm discrepancy for **2** and 48 ppm for **3**. The agreement of the chemical shifts for the other carbons with experiment is about the same for **1** and **2**, with each carbon within the (ca. 10 ppm) error range normally given by IGLO DZ for hydrocarbons.[9c] The average discrepancies for C1, C3, and C4 are 5.0 ppm for **1**, 3.4 ppm for **2**, and 8.5 ppm for **3**.

Table II. DZ IGLO Chemical Shifts (vs CH$_4$)[a] of *tert*-Pentyl and 1-Propyl Cations as a Function of the CH$_3$–CH$_2$–C$^+$ Angle

descriptn	angle[b] C–C–C$^+$	δ_C, ppm C1	C2	C3	C4
exptl[c] *tert*-pentyl		44.6	335.4	57.5	9.3
1[d]	101.5	41.9	335.7	49.9	14.1
1[e]	106.3	44.0	357.3	48.2	12.1
1[f]	68	25.4	143.3	120.8	23.6
1[f]	88	36.6	294.8	59.0	14.2
1[f]	98	41.1	337.7	51.6	14.3
1[g]	104.8	42.8	353.0	49.8	15.1
1[f]	108	43.9	358.3	48.0	15.9
1[f]	118	45.5	366.9	46.3	18.3
2[d]	119.5	43.9[h]	352.9	49.9	7.3
2[e]	119.0	44.7[h]	365.9	50.9	6.3
3[d]	91.6	36.4	287.2	47.3	2.3
3[e]	103.4	42.5	343.5	42.9	4.3
n-propyl[f]	68	111.5	124.3	9.9	
n-propyl[f]	78	170.6	87.6	13.4	
n-propyl[f]	88	236.5	68.1	16.1	
n-propyl[f]	98	292.6	58.9	21.6	
n-propyl[f]	108	328.0	54.6	28.4	
n-propyl[f]	118	343.5	52.8	34.2	
n-propyl[g,i]	117.3	352.9	58.1	8.5	
n-propyl[g,j]	69.2	117.8	117.8	10.0	

[a] The DZ-calculated IGLO chemical shifts for CH$_4$ and for TMS are practically identical. [b] Angles in degrees. [c] Reference 1c; experimental vs TMS. [d] Fully optimized geometry at MP2/6-31G* level. [e] Fully optimized geometry at 6-31G* level. [f] Geometry optimized at the HF/3-21G level but C–C–C$^+$ angle fixed. [g] Fully optimized geometry at 3-21G level. [h] Average values. [i] "In-plane" C_s geometry. [j] Corner-protonated cyclopropane.

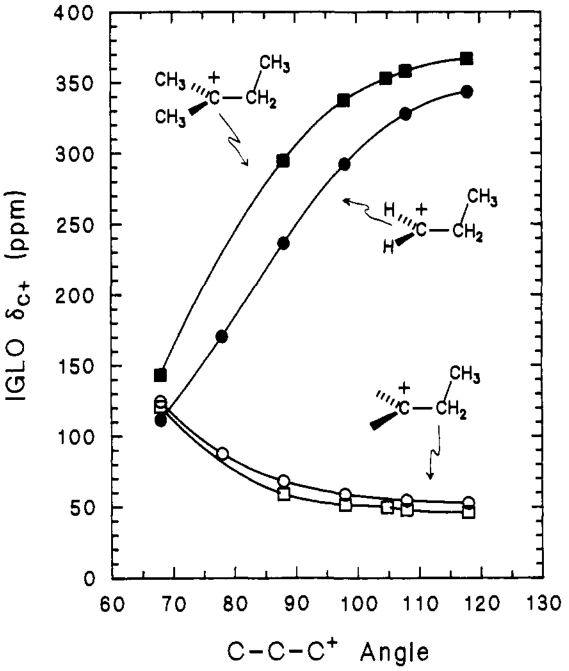

Figure 1. The dependence of ^{13}C chemical shifts (IGLO DZ//3-21G calculations) on the CH$_3$–CH$_2$–C$^+$ angle. The upper curves are for C$^+$ in **1** (■) and the 1-propyl (●) cation, and the lower curves are for the CH$_2$ carbons in **1** (□) and the 1-propyl (○) cation. See Table II for the data plotted.

Hyperconjugation is evident in **1** from the lengthening of the C3–C4 bond to 1.58 Å. However, particularly noteworthy is the C4–C3–C2$^+$ angle of 101.5° calculated for **1**, clearly indicating distortion of the C–C hyperconjugating form toward bridging.

---

(7) (a) Gaussian 82, CRAY Version K: Binkley, J. S.; Frisch, M. J.; DeFrees, D. J.; Raghavachari, K.; Whitesides, R. A.; Schlegel, H. B.; Fluder, E. M.; Pople, J. A., Department of Chemistry, Carnegie-Mellon University, Pittsburgh, PA; modified by Convex for the C1 computer in Erlangen. (b) Gaussian 86, Vectorized IBM Version: Frisch, M. J.; Binkley, J. S.; Schlegel, H. B.; Raghavachari, K.; Melius, C. F.; Martin, R. L.; Stewart, J. J. P.; Bobrowicz, F. W.; Rohlfing, C. M.; Kahn, L. R.; DeFrees, D. J.; Seeger, R.; Whitesides, R. A.; Fox, D. H.; Fluder, E. M.; Pople, J. A., Carnegie-Mellon University, Pittsburgh, PA.

(8) For a description of basis sets and standard procedures, see: Hehre, W. J.; Radom, L.; Schleyer, P. v. R.; Pople, J. A. *Ab Initio Molecular Orbital Theory*; Wiley-Interscience: New York, 1987.

(9) (a) Kutzelnigg, W. *Isr. J. Chem.* **1980**, *19*, 193. (b) Schindler, M.; Kutzelnigg, W. *J. Chem. Phys.* **1982**, *76*, 1919. (c) Schinlder, M.; Kutzelnigg, W. *J. Am. Chem. Soc.* **1983**, *105*, 1360.

Figure 1 shows how strongly the C4–C3–C2$^+$ angle influences the chemical shifts, particularly for C2$^+$, but also for C3 in **1**. When the C4 methyl is in a fully bridging position (68° CCC$^+$ angle) the chemical shifts of C2 and C3 become nearly equal (Figure 1 and Table II). Figure 1 also includes plots of data for the 1-propyl cation (summarized in Table II) constrained to various CCC$^+$ angles. The 1-propyl cation is not an experimentally observable species, but the IGLO results show that the influence of the degree of bridging on the local electronic environment of the cation center and adjacent nucleus appears to be general. The strong dependence on extent of bridging is also evident in the IGLO calculations for **3**, where a change of about 12° in CCC$^+$ angle produces a 56 ppm change at C2$^+$.

Previous IGLO calculations[10] on CH_3^+, and all secondary and tertiary carbocations calculated with classical geometries (from small ab initio basis sets), predict nearly identical carbon shifts of 360–370 ppm for C$^+$, which are far from the more shielded values of 320–340 ppm considered typical of classical cations.[11] However, very good matches of theoretical to experimental ^{13}C shifts for secondary and tertiary carbocations can be achieved following geometry optimizations with extended basis sets.[10] It is now clear that the strong dependence of the IGLO DZ calculated shifts on the basis sets used for geometry optimization is primarily due to the degree of bridging, since similar IGLO predictions (Table II) are obtained from 3-21G, 6-31G*, or MP2/6-31G* geometries, as long as the C–C–C$^+$ angle is similar. The lower levels of theory do not give fully optimized structures with enough bridging, by either carbon or hydrogen. Hence, even one of the simplest representatives of tertiary alkyl carbocations, the *tert*-pentyl cation, is not fully classical: partial bridging alters the local electronic structure sufficiently to shield C$^+$ and give the observed shift of 335.7 ppm. If there is any dynamic averaging in the *tert*-pentyl cation involving **2** and **3** as well as **1**, it is clear that the equilibrium must be dominated by partially bridged species to reach this observed shift.

The success of matching calculated and experimental chemical shifts, generally within ±10 ppm,[10] in part is its own justification for comparing theoretical (gas-phase) predictions with solution measurements. Further justification comes from the remarkable constancy shown by the chemical shifts of carbocations as long as the medium is sufficiently nonnucleophilic to support their existence. For example, an examination of the *tert*-pentyl cation prepared from the chloride in six different solvents of varying nucleophilicity and with both SbF_5 and AsF_5-based counterions found no evidence for nucleophilic interaction by solvent or counterion.[1d] The chemical shifts at all positions varied with conditions, but all variations were within a range of 2.5 ppm, and preparation from the alcohol in FSO_3H/SbF_5 gave similar shifts. The small shift variation at C$^+$ tracked very well with the changes at C$^+$ in the *tert*-butyl cation,[1d] so the variation cannot be attributed to varying populations of **1** and **2** with differential solvation. However, it is possible that solvation plays a role in the energy difference between **1** and **2** in solution. Solvent and counterion have been noted to have some influence on closely balanced structural equilibria in carbocations,[12] and NMR relaxation measurements suggest that solvation influences the rate of reorientation of carbocations in solution.[13]

The high sensitivity of the chemical shifts to the CCC$^+$ angle (ca. 6 ppm/deg from 68° to 98°) as shown in Figure 1 may also help explain observations of large intrinsic NMR isotope shifts in some carbocations upon substitution of deuterium for protium, particularly in those cases where partial bridging is well developed. For example, it was previously suggested that the large isotope shifts at C2$^+$ and C1 in the 2-methyl-2-norbornyl cation were due to perturbation of the degree of bending along the bridging coordinate for C2–C1–C6.[14] It is now obvious from Figure 1 that only slight changes in bond angles associated with bridging in carbocations produce large changes in chemical shifts.

Acknowledgment. This work was supported at Erlangen by the Stiftung Volkswagenwerk, the Fonds der Chemischen Industrie, and the Convex Computer Corporation. We also thank Prof. W. Kutzelnigg and his Bochum group particularly for the development of the IGLO program and Dr. M. Schindler for the Convex version. We also thank Prof. W. J. Hehre for providing facilities and advice and IBM Düsseldorf for providing computational facilities on which the higher level calculations were carried out. J.W.d.M.C. thanks CNPq-Brazil for financial support through a doctoral fellowship.

Supplementary Material Available: Table of the absolute energies of 2-methyl-2-butyl cation isomers and table of MP2-(FU)/6-31G* geometries (2 pages). Ordering information is given on any current masthead page.

---

[10] (a) Schindler, M. *J. Am. Chem. Soc.* **1987**, *109*, 1020. (b) Bremer, M.; Schleyer, P. v. R.; Schotz, K.; Kausch, M.; Schindler, M. *Angew. Chem.* **1987**, *99*, 795; *Angew. Chem., Int. Ed. Engl.* **1987**, *26*, 761. (c) Schleyer, P. v. R.; Laidig, K.; Wiberg, K. B.; Saunders, M.; Schindler, M. *J. Am. Chem. Soc.* **1988**, *110*, 300. (d) Laidig, K.; Saunders, M.; Wiberg, K. B.; Schleyer, P. v. R. *J. Am. Chem. Soc.* **1988**, *110*, 7652. (e) Bremer, M.; Schleyer, P. v. R.; Fleischer, U. *J. Am. Chem. Soc.* **1989**, *111*, 1147. (f) Koch, W.; Liu, B.; Schleyer, P. v. R. *J. Am. Chem. Soc.* **1989**, *111*, 3479. (g) Schleyer, P. v. R.; Koch, W.; Liu, B. Fleischer, U. *J. Chem. Soc., Chem. Commun.* **1989**, 1098. (h) Schleyer, P. v. R.; Carneiro, J. W. de M.; Koch, W.; Raghavachari, K. *J. Am. Chem. Soc.* **1989**, *111*, 5475. (i) Carneiro, J. W. de M.; Schleyer, P. v. R.; Koch, W.; Raghavachari, K. *J. Am. Chem. Soc.* **1990**, *112*, 4064.

[11] Kirchen, R. P.; Okazawa, N.; Ranganayakulu, K.; Rauk, A.; Sorensen, T. S. *J. Am. Chem. Soc.* **1981**, *103*, 597.

[12] (a) Kirchen, R. P.; Sorensen, T. S. *J. Am. Chem. Soc.* **1978**, *100*, 1487. (b) Kirchen, R. P.; Ranganayakulu, K.; Sorensen, T. S. *J. Am. Chem. Soc.* **1987**, *109*, 7811.

[13] Kelly, D. P.; Leslie, D. R. *J. Am. Chem. Soc.* **1990**, *112*, 9078.

[14] (a) Forsyth, D. A.; Botkin, J. H.; Puckace, J. S.; Servis, K. L.; Domenick, R. L. *J. Am. Chem. Soc.* **1987**, *109*, 7270. (b) Forsyth, D. A.; Panyachotipun, C. *J. Chem. Soc., Chem. Commun.* **1988**, 1564.

Direct Observation of Hot Vibrations in Photoexcited Deoxyhemoglobin Using Picosecond Raman Spectroscopy

Robert Lingle, Jr.,[†] Xiaobing Xu, Huiping Zhu,
Soo-Chang Yu, and J. B. Hopkins*

Department of Chemistry, Louisiana State University
Baton Rouge, Louisiana 70803

K. D. Straub

John L. McClellan VA Hospital
Little Rock, Arkansas 72205

Received December 6, 1990

We present the first study of the hot vibrational population in a photoexcited heme protein *directly* observed in the picosecond anti-Stokes Raman spectrum. Time-resolved resonance Raman scattering selectively probes strongly enhanced vibrations of the porphyrin chromophore and provides specific information on the population of excited vibrations. Our pump–probe Raman experiment with 8-ps time resolution unambiguously detects the excited vibrational levels of deoxyhemoglobin (deoxyHb) which are populated following optical excitation. Assuming thermal distribution of vibrational energy, we estimate a vibrational temperature of 36 K above room temperature within our 8-ps resolution. The 1/*e* time constant for vibrational cooling is 2–5 ps.[1]

Several attempts have been made to characterize the ultrafast dynamics of vibrational energy dissipation in photoexcited heme proteins.[2-4] Previous Raman experiments were unable to probe

---

[†] Department of Physics and Astronomy, LSU.

[1] Picosecond dynamics data, to be published.

[2] Petrich, J. W.; Martin, J. L.; Houde, D.; Poyart, C.; Orzag, A. *Biochemistry* **1987**, *26*, 7914.

[3] Anfinrud, P. A.; Han, C.; Hochstrasser, R. M. *Proc. Natl. Acad. Sci. U.S.A.* **1989**, *86*, 8387.

0002-7863/91/1513-3992$02.50/0